Journal of Catalysis 273 (2010) 211–220

Contents lists available at ScienceDirect

Journal of Catalysis

journal homepage: www.elsevier.com/locate/jcat

Mediatory role of tin in the catalytic performance of tailored platinum–tin alloy surfaces for carbon monoxide oxidation

Céline Dupont [a,b], Yvette Jugnet [b], Françoise Delbecq [a], David Loffreda [a,*]

[a] Université de Lyon, Institut de Chimie de Lyon, Laboratoire de Chimie, UMR CNRS 5182, Ecole Normale Supérieure de Lyon, 46 Allée d'Italie, F-69364 Lyon Cedex 07, France
[b] Université Lyon 1, Institut de Recherches sur la Catalyse et l'Environnement de Lyon, UMR CNRS 5256, 2 Avenue Albert Einstein, F-69626 Villeurbanne Cedex, France

ARTICLE INFO

Article history:
Received 2 March 2010
Revised 19 May 2010
Accepted 22 May 2010
Available online 1 July 2010

Keywords:
Carbon monoxide
Oxidation
Oxygen
Dissociation
Platinum
Tin
Alloy
Kinetic
Density functional theory

ABSTRACT

The activation of oxygen reduction reaction fascinates numerous scientists in the fields of heterogeneous catalysis, electrochemistry and surface science. Indeed, oxygen dissociation is considered usually as the rate determining step of several reactions on conventional platinum catalysts. From combined experimental and theoretical approaches, we demonstrate comprehensively how tailored platinum–tin alloy surfaces allow to go beyond this chemical limitation. Near-ambient pressure kinetic measurements show the outstanding capacity of the $Pt_3Sn(1\,1\,1)$ single-crystal surfaces for carbon monoxide oxidation. The apparent activation energy is almost twice lower on the platinum–tin surface than on pure platinum catalyst. The theoretical analysis based on density functional theory calculations supports the idea that oxygen dissociation is never the rate determining step on these alloy surfaces since the corresponding rates calculated at room temperature always outstrip those of carbon monoxide oxidation. The influence of surface tin content and oxygen coverage on the activity is addressed in details. The mediatory role of tin in the alloy is elucidated on the basis of a charge transfer analysis.

1. Introduction

The elucidation of the role of the catalyst on kinetics is an everyday challenge in chemistry. Although tremendous experimental and theoretical efforts are conceded to solve this question on specific reactions, our current understanding is rarely sufficient to allow the design of new catalytic materials, offering enhanced properties. Oxygen activation is a probative example. Due to the strong industrial implications in heterogeneous catalysis and in biochemistry, oxygen dissociation is often examined on noble and coinage metals and frequently evoked as a critical step for a large family of oxidation reactions [1–3]. In particular for fuel cell (FC) industry, the lowering of the cathodic overpotential linked to the oxygen reduction reaction (ORR) remains a constant challenge [4–6]. In addition, the control of the anodic carbon monoxide poisoning ruled by oxygen activation is not ensured yet. These investigations thus show undeniably our limits concerning the understanding of kinetics of the catalyst and consequently those regarding the conception of more efficient materials.

In heterogeneous catalysis, regular transition metals such as Pt and Pd are usually employed for oxidation reactions, involving oxygen dissociation. In the recent years, tremendous efforts have been oriented toward the understanding of the active phase of the catalyst surface for carbon oxidation reaction, especially for pure late transition metals (Ru, Pt, Pd and Rh). Several experimental and theoretical groups have tackled the key question of the formation of a surface oxide (such as RuO_2, PtO_2, PdO and RhO_2) in the reaction conditions [7–16]. However, the oxygen dissociation elementary step exhibits a significant activation energy barrier, according to theory [17,18]. Different solutions could be proposed for overcoming this technological issue. O_2 activation could be improved either by modifying the catalyst morphology (particles, steps, kinks, defects,...), or by changing the chemical composition of the catalytic material (bimetallics, supported particles or bioenzymes,...). For instance, bimetallics such as PtRu, PtMo and PtSn catalysts have been evoked in the literature for solving the question of CO tolerance for FC industrial applications [19,20].

From the experimental point of view, various bimetallic materials have been examined for their catalytic properties toward CO oxidation [21–28]. However, a kinetic investigation (apparent kinetic rate constants and activation energies) demonstrating the efficiency gain is rarely proposed [26,29]. Generally, a mechanistic

* Corresponding author. Fax: +33 4 72 72 88 60.
E-mail address: david.loffreda@ens-lyon.fr (D. Loffreda).
URL: http://perso.ens-lyon.fr/david.loffreda (D. Loffreda).

0021-9517/$ - see front matter © 2010 Elsevier Inc. All rights reserved.
doi:10.1016/j.jcat.2010.05.014

scheme is postulated without a clear basement (bifunctional mechanism, site blocking, etc.).

From the theoretical point of view, the key role of the second metal in bimetallics is often explained either through a d-band model (d-band shifts) or through an electronic analysis of the adsorbed state (electronic ensemble and ligand effects) [30–33]. The reaction pathways of oxygen reduction reaction and of CO oxidation are usually explored by state-of-the-art density functional theory (DFT) calculations [20,34–40]. However, the role of the secondary metal on kinetic properties is rarely elucidated from these atomistic approaches by a detailed electronic analysis and charge transfer at the transition states.

In this context, O_2 dissociation linked to CO oxidation on PtSn catalysts is a probative example where those experimental and theoretical limitations still hold. Indeed, this catalytic system exhibits an enhanced catalytic performance compared to pure Pt reference [22,24]. In this work, we aim at elucidating the key role of tin on kinetics of O_2 dissociation and CO oxidation on $Pt_3Sn(1\,1\,1)$ surfaces. The demonstration relies on a joint experimental and theoretical investigation. The tin content and the oxygen coverage effects on the catalyst activity are addressed. Kinetic rate constants at different temperatures and apparent activation energies are determined by experimental studies performed at elevated pressure of reactants. A mechanistic study including kinetic rate constants and activation barriers is proposed by an atomistic DFT approach. The question of the role of the secondary metal (tin) on kinetics is solved by charge transfer and Mulliken population analyses. The tin content and the oxygen coverage effects are explained by an energetic decomposition model.

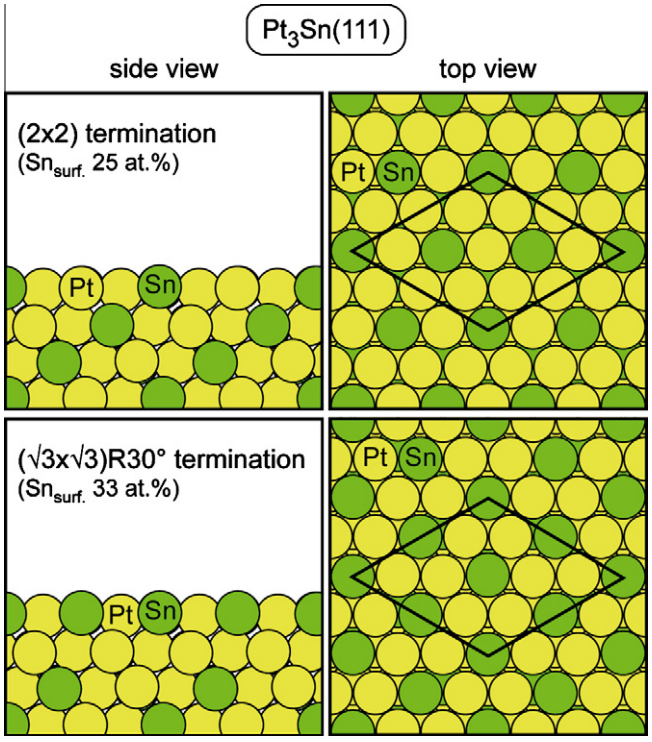

Fig. 1. Top and side views of $Pt_3Sn(1\,1\,1)$-(2×2) and $Pt_3Sn(1\,1\,1)$-$\left(\sqrt{3}\times\sqrt{3}\right)R30^\circ$ terminations. The definition of the $\left(2\sqrt{3}\times2\sqrt{3}\right)$ unit cells (1/12 ML) is reported.

2. Methodology

2.1. Experimental details

CO oxidation experiments are performed in a special cell, which is described in details previously [41,25] so that only a short description is given here. Briefly, this cell (about 1 L volume) is a bakeable stainless steel chamber designed for measurements in a wide range of pressure from ultra high vacuum (UHV) to ambient pressure. Under a PM-IRRAS (polarization modulation reflection absorption infrared spectroscopy) environment, this reaction cell is also attached to a UHV chamber devoted to sample preparation and surface characterization.

The $Pt_3Sn(1\,1\,1)$ sample (8 mm diameter, 1 mm thick) is prepared by conventional UHV procedures inside the preparation chamber equipped with ion sputtering, electron bombardment, quadrupole mass spectroscopy (QMS – Transpector 2 from Inficon) and X-ray photoelectron spectroscopy (XPS – VSW HA50 with a dual Al–Mg X-ray source). The (2×2) and the $\left(\sqrt{3}\times\sqrt{3}\right)R30^\circ$ $Pt_3Sn(1\,1\,1)$ surfaces are prepared by a series of Ar^+ sputtering and 20 min annealing at 1100 K and 600 K, respectively, following Bardi et al. protocol [42,43]. The tin surface concentration is 25 at.% and 33 at.% for the (2×2) and the $\left(\sqrt{3}\times\sqrt{3}\right)R30^\circ$, respectively (see Fig. 1). The Pt(1 1 1) reference sample (10 mm diameter, 1 mm thick) is prepared by series of ion sputtering and 5 min annealing to 1100 K. From time to time, between two series of sputtering-annealing, an oxidation step (10^{-7} Torr O_2, 900 K, 5 min) is performed in order to remove residual carbidic contamination induced by previous CO oxidation reactions. The samples are cleaned until no impurity is detected by XPS. The tin concentrations are determined from the Pt4f and Sn3d photoelectron spectra measured along the normal to the surface. These concentrations, integrated over the whole analyzed depth, are estimated to 25 at.% and 16.5 at.% for the (2×2) and the $\left(\sqrt{3}\times\sqrt{3}\right)R30^\circ$ $Pt_3Sn(1\,1\,1)$ surfaces, respectively. Hence, they clearly indicate a depletion of tin in the sublayers of the $\left(\sqrt{3}\times\sqrt{3}\right)R30^\circ$ $Pt_3Sn(1\,1\,1)$ surface, in agreement with Bardi et al. [42,43]. Once prepared and characterized by XPS, the samples are transferred under UHV into the reaction cell.

All reactions are studied following the same approach. Carbon monoxide is introduced first, then O_2 is added in the reactor at room temperature, and the sample is progressively heated to the required temperature. Before introduction into the reaction cell, CO gas (Linde 3.7) is passed through a molecular sieve (5A 4–8) and then through a liquid nitrogen trap in order to prevent any Ni carbonyl adsorption and further decomposition on the surface. The CO gas container is equipped with a Ni free valve. O_2 gas (alphagas N55) is only passed through a liquid nitrogen trap.

The activity of the sample is monitored by mass spectroscopy after successive gas samplings (at 10^{-6} Torr) from the reactor through a leak valve. The curves of partial pressures P_{CO}, P_{O_2} and P_{CO_2} are calculated from the evolution of masses linked to CO ($m/e = 28$), O_2 ($m/e = 32$) and CO_2 ($m/e = 44$). Pure CO, O_2 and CO_2 gases are used for calibrating the mass spectra. The pressure inside the reactor is monitored with a membrane gauge.

2.2. Computational details

The theoretical study is based on density functional theory calculations in periodic boundary conditions with VASP [44,45]. The general gradient approximation (GGA) is used with Perdew–Burke–Ernzerhof (PBE) [46] exchange correlation functional and the projector augmented-wave (PAW) [47] method. The Kohn–Sham one-electron equations are solved on the basis of plane wave with kinetic energies below 400 eV. A $\left(2\sqrt{3}\times2\sqrt{3}\right)$ supercell describes the two existing terminations of the $Pt_3Sn(1\,1\,1)$ surface, as drawn in Fig. 1. Non-symmetric metallic slabs composed of five layers are considered with a vacuum of 14 Å. In order to describe

correctly the experimental layer-by-layer Pt and Sn atomic concentrations [42,43], a Pt_3Sn stoichiometry is respected in each layer with a (2×2) arrangement for the $Pt_3Sn(111)$-(2×2). For the $Pt_3Sn(111)$-$\left(\sqrt{3} \times \sqrt{3}\right)R30^\circ$, the PtSn concentration ratio is respected in the complete slab. The increase in tin content in the surface layer (Pt_2Sn) is counterbalanced by a tin depletion in the second plane (Pt_5Sn) [48], in agreement with experiments [42]. Adsorbates are deposited only on one side of the slab. In the geometry optimizations, all the degrees of freedom of adsorbates and those of the three uppermost metal layers are relaxed. The two lowest metallic planes are frozen in a bulk-like geometry with the optimized parameter (2.876 Å). The Brillouin zone integration is performed on a $(3 \times 3 \times 1)$ Monkhorst–Pack k-point mesh. The numerical error on the total electronic energy is lower than 0.01 eV.

The technique for the vibrational analysis is based on the numerical calculation of the second derivatives of the potential energy surface within the harmonic approach, as detailed previously [40].

The minimization of the reaction pathways and the search of the transition states (TS) are performed by the climbing-image nudged elastic band method (CI-NEB) [49,50]. The obtained TS geometry is further refined by a quasi-Newton algorithm, and the saddle point is characterized by a single imaginary frequency.

Spin polarization effects are considered for molecular oxygen adsorption as exposed previously [48], although the stabilizing effect is rare. For the complex study of reactivity, only spin restricted calculations have been considered.

The calculation of the effective rate constant $k^{eff}(T)$ is derived from the product of the rate constant $k(T)$ following the transition-state theory and the diffusion equilibrium constant K_{dif} with usual approximations:

$$k^{eff}(T) = k(T)K_{dif} = k^0(T)e^{\left(\frac{-\left(E_{act}^{ZPE}+\Delta E_{dif}\right)}{k_BT}\right)} \quad (1)$$

$$= \frac{k_BT}{h}\frac{Q_{TS}}{Q_{IS}}e^{\left(\frac{-\left(E_{act}^{ZPE}+\Delta E_{dif}\right)}{k_BT}\right)} = k^0(T)e^{\left(\frac{-E_{act}^{eff}}{k_BT}\right)} \quad (2)$$

$k^0(T)$ is the pre-exponential factor including the total partition functions for the initial state Q_{IS} and the transition state Q_{TS}. E_{act}^{ZPE} is the activation energy including zero-point energy (ZPE) corrections. ΔE_{dif} is the diffusion energy between the most stable adsorption structure and the dissociation precursor state. E_{act}^{eff} is the effective activation energy. The definition of adsorption states and their corresponding energies are illustrated for O_2 dissociation in Fig. 2. For carbon monoxide oxidation, ΔE_{dif} equals zero since no diffusion phenomenon occurs.

The Mulliken population analyses are calculated with the DMol3 package [51] from VASP optimized structures.

3. Experimental observation

The carbon monoxide oxidation is investigated on the two terminations of $Pt_3Sn(111)$ and on $Pt(111)$ for a direct comparison. A first set of experiments is run on the three surfaces with constant temperature, total pressure and P_{CO}/P_{O_2} reactant pressure ratio. The catalytic activities are compared in these conditions. Then, the temperature influence on the CO_2 formation rate is measured in order to evaluate the apparent activation energy. The results are reported in Fig. 3.

In order to check the stability of the PtSn alloy surface terminations and to rule out the formation of a complete surface monolayer of tin oxide, standard X-ray photoelectron spectroscopy measurements are taken before and after the reaction. No significant change in the electronic signatures of surface tin is observed. In addition, when a consecutive series of catalytic tests is performed on the same surfaces, the performances are well reproduced. Hence, these observations are in favor of stable PtSn bimetallic alloy surfaces in the explored range of temperature (300–425 K), in agreement with Atrei et al.'s study which indicates that a high temperature is required to form a complete surface oxide (800 K at 10^{-6} mbar) [52].

The evolution of the CO_2 partial pressure with time during the reaction at 425 K is reported in the inset of Fig. 3 for the three surfaces. 10^{-1} Torr CO followed by 1 Torr O_2 is introduced in the reac-

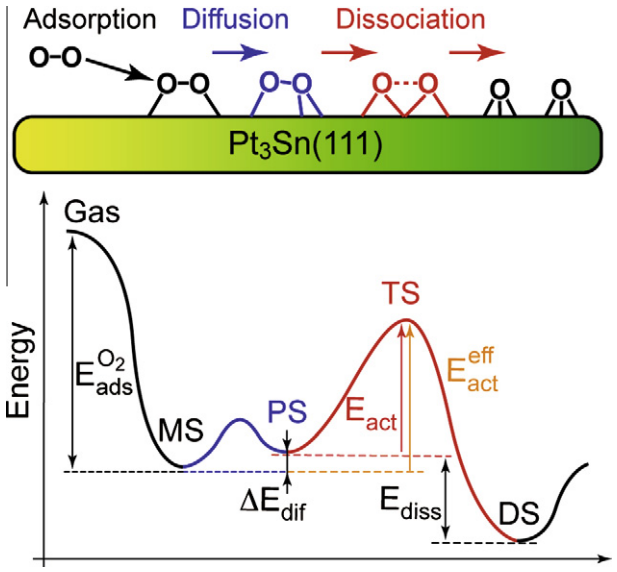

Fig. 2. Energy scheme for O_2 dissociation on the $Pt_3Sn(111)$ surfaces. MS is the molecular oxygen thermodynamic state. PS corresponds to the molecular precursor state before dissociation. TS is the dissociation transition state. DS is the atomic oxygen dissociated state. $E_{ads}^{O_2}$ is the adsorption energy of MS. ΔE_{dif} is the diffusion energy between MS and PS. E_{act} is the dissociation activation barrier. E_{act}^{eff} is the effective activation energy including the diffusion energy ΔE_{dif}. E_{diss} is the dissociation energy between PS and DS.

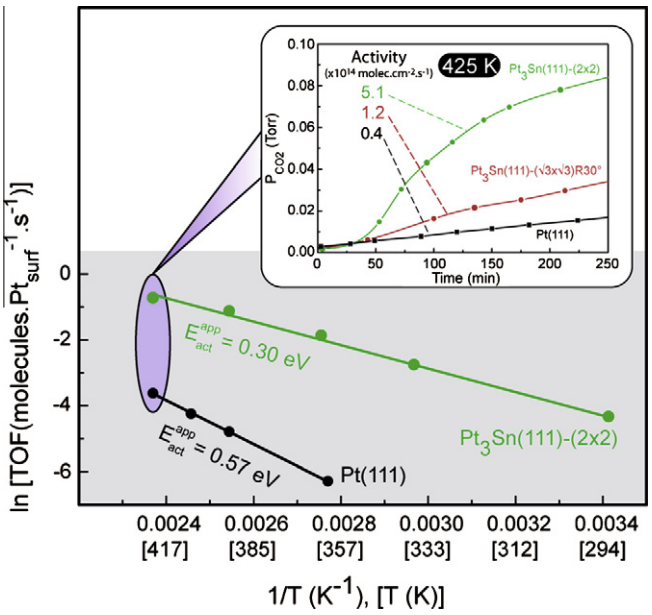

Fig. 3. Comparative Arrhenius plots for CO oxidation on $Pt_3Sn(111)$-(2×2) and $Pt(111)$. Each TOF value results from one activity curve, such as those addressed in the inset at 425 K for $Pt_3Sn(111)$-(2×2), $Pt_3Sn(111)$-$\left(\sqrt{3} \times \sqrt{3}\right)R30^\circ$ and $Pt(111)$ (Pt_{surf} refers to the number of surface Pt atoms). The experimental conditions are V_{reac} = 1 L and P_{reac} = 1.1 Torr with $PO_2/P_{CO} = 10$.

tor at 300 K. Zero reference on the time scale corresponds to the moment when oxygen is introduced and when heating is started. A first mass spectrum is recorded within the first few minutes in order to determine the accurate initial reactant ratio. Twenty-five minutes are necessary to reach the required temperature (425 K in that case). The activity is calculated as follows (see all the details in the Supplementary information):

$$A = \frac{1.606 \times 10^{20}}{S} \times \frac{V_{reac}}{T_{reac}} \times \frac{\Delta P}{\Delta t} \quad (3)$$

with A the activity per surface unit area (mol cm^{-2} s^{-1}), S the sample area (0.5 cm^2 and 0.785 cm^2 for $Pt_3Sn(1\,1\,1)$ and $Pt(1\,1\,1)$ samples, respectively), V_{reac} the volume of the reactor (1.0 L), T_{reac} the reactor temperature (K) and $\Delta P/\Delta t$ the slope of the curve $P_{CO_2} = f(t)$ (Torr min^{-1}). In this work, the activity is systematically determined for conversion rates lower than 50%.

The calculated activities are determined at 425 K with a total pressure of 1.1 Torr and a P_{O_2}/P_{CO} ratio set at 10. At this temperature, clear differences are observed between the three surfaces. First, alloying platinum with tin makes the $Pt_3Sn(1\,1\,1)$ surface about one order of magnitude more efficient than $Pt(1\,1\,1)$ for the production of CO_2. Second, the surface tin concentration affects the performance of the catalyst. In fact, the (2×2) termination, which exhibits a lower tin content, is four times more active than the $\left(\sqrt{3} \times \sqrt{3}\right)R30^\circ$ surface.

In order to go further and determine the activation energy of the reaction, several curves of this type have to be obtained at different temperatures and on the different samples. It is worth noting that the $\left(\sqrt{3} \times \sqrt{3}\right)R30^\circ$ termination has not shown a significant activity at 300 K. This explains why this surface has not been investigated with more efforts. In Fig. 3, the variation of activity is reported as a function of temperature for the most active $Pt_3Sn(1\,1\,1)$-(2×2) termination and for $Pt(1\,1\,1)$, used as reference. The activities are now expressed in terms of turnover frequency (TOF) defined as the number of CO_2 molecules produced by active site and by time unit:

$$TOF = \frac{A}{N_{Pt}} \quad (4)$$

with N_{Pt} the number of Pt atoms per surface unit (1.46×10^{15} and 1.05×10^{15} Pt atoms cm^{-2} for $Pt(1\,1\,1)$ and $Pt_3Sn(1\,1\,1)$-(2×2), respectively). In our definition, only the surface Pt atoms are considered since we have demonstrated previously from high resolution electron energy loss spectroscopy measurements and DFT calculations that CO does not adsorbs on surface Sn atoms [40,53]. It is worth noting that the $\left(\sqrt{3} \times \sqrt{3}\right)R30^\circ$ has not shown a significant activity at 300 K. This explains why it has not been investigated with more efforts.

The plots ln(TOF) as a function of inverse temperature (1/K) are linear in the studied temperature range and obey an Arrhenius law. The apparent activation energies, E_{act}^{app}, are deduced from the slope of these Arrhenius plots, as follows:

$$E_{act}^{app} = R \times \frac{\Delta ln(TOF)}{\Delta(1/T)} \quad (5)$$

The apparent activation energy reflects the whole reaction mechanism involving the elementary steps of O_2 dissociation and CO oxidation. The calculated barriers are 0.30 and 0.57 eV for $Pt_3Sn(1\,1\,1)$-(2×2) and $Pt(1\,1\,1)$, respectively. Hence, the increase in the activity observed at 425 K on $Pt_3Sn(1\,1\,1)$-(2×2) is related to a significant decrease in the apparent activation energy. These results are fully compatible with those published previously by Schubert and coworkers [22]. In fact, the authors have obtained apparent barriers of 0.32 and 0.79 eV on Pt_3Sn and Pt supported particles, respectively. Moreover, our estimated barrier on $Pt(1\,1\,1)$ (0.57 eV) agrees with previous results (0.53–0.67 eV) [54,55].

4. Theoretical analysis

The experimental observation has demonstrated undeniably a strong catalytic activity of $Pt_3Sn(1\,1\,1)$ surfaces for CO oxidation. However, since only the apparent activation energy has been measured, the specific role of tin on each elementary step, O_2 dissociation and CO oxidation, is not elucidated yet. In fact, identifying the nature of a general mechanism in heterogeneous catalysis is actually challenging. To go beyond such a limitation, theoretical approaches can provide a substantial understanding by describing atomistic thermodynamics and kinetics of the elementary acts. According to a previous theoretical investigation into CO oxidation on $Pt(1\,1\,1)$ [56], a concerted mechanism through molecular oxygen may coexist with a stepwise process through a preliminary oxygen dissociation. The preferential route depends partly on the oxygen and carbon monoxide respective coverage. At low coverage (1/8 ML), the concerted mechanism is favored, while at higher coverage (1/4 ML), oxygen dissociation follows a stepwise pathway. In our study, the picture is more complex since tin directly changes the catalytic activity. In the following section, the influence of tin on the possible mechanisms will be explored on $Pt_3Sn(1\,1\,1)$ at a low coverage (1/12 ML).

4.1. Oxygen dissociation

The elaboration of the dissociation pathways requires a previous investigation of molecular oxygen adsorption states. The chemisorption study has been proposed before on the $Pt_3Sn(1\,1\,1)$ surfaces [48]. The picture is different on the (2×2) and $\left(\sqrt{3} \times \sqrt{3}\right)R30^\circ$ terminations. On the former, molecular oxygen interacts preferentially with two surface Pt atoms through a top–top position (see α in Fig. 4), whereas on the latter, the adsorbate sits on a Pt_2Sn hollow site (see γ in Fig. 4). The adsorption energy is smaller on the $\left(\sqrt{3} \times \sqrt{3}\right)R30^\circ$ termination. On the (2×2), the dissociation pathway starting from the α thermodynamic adsorption structure is not direct. Two preliminary migration pathways exist (cf. Figs. 2 and 4). The first one (m_1) leads to a metastable precursor state β_1 in which the oxygen molecule sits in a pure Pt_3 hollow site, whereas the second pathway (m_2) gives a precursor state β_2 where the molecule is bonded to the surface through a mixed Pt_2Sn hollow site. In the latter case, the diffusion is a multistep process involving four different molecular adsorption structures, as depicted in the figure ($T_{Pt}T_{Pt}(Sn_{hcp})$, $T_{Pt}B_{PtSn}(Pt_{fcc})$, $T_{Pt}T_{Sn}$, $T_{Pt}B_{PtSn}(Pt_{hcp})$).

The precursor states β_1 and β_2 correspond to the initial states of the possible dissociation pathways which are defined throughout the article as 25%-Pt_3 and 25%-Pt_2Sn, respectively, in agreement with the chemical nature of the adsorption site and the surface tin content of the termination. In the case of $\left(\sqrt{3} \times \sqrt{3}\right)R30^\circ$, only one dissociation pathway exists (noted 33%-Pt_2Sn) starting from γ initial state. According to our definition in Fig. 2, molecular and precursor states are thus identical. The results regarding the fine minimization of the reaction pathways have been summarized in Fig. 5 and in Table 1.

On $Pt_3Sn(1\,1\,1)$-(2×2) as exposed in Fig. 5, the two possible pathways exhibit similar initial (IS) and final (FS) structures. They differ only by the chemical nature of the interacting metal atoms. In contrast, the transition states (TS) are geometrically different. The 25%-Pt_3 pathway leads to a dissociation through an asymmetric TS (one oxygen atom on a top position, while the other one on a bridge site), whereas the second 25%-Pt_2Sn route exhibits an

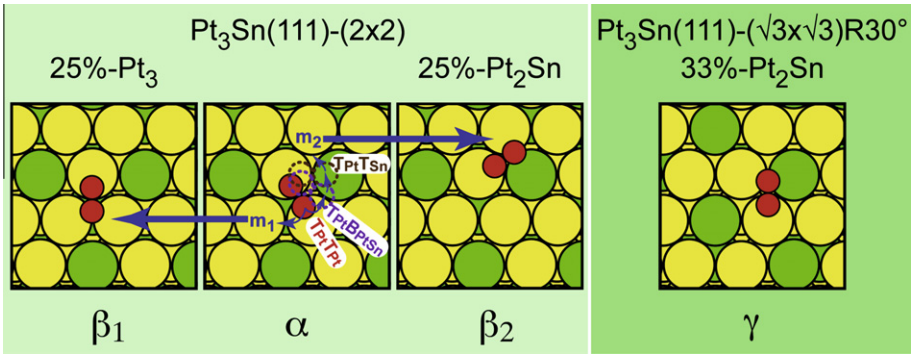

Fig. 4. Precursor states of molecular oxygen adsorption on $Pt_3Sn(1\,1\,1)$-(2×2) and on $Pt_3Sn(1\,1\,1)$-$\left(\sqrt{3}\times\sqrt{3}\right)R30^\circ$. For the (2×2) termination, the obtained migrations (m_1 and m_2) from the most stable adsorption structure (α) to metastable precursor states for dissociation (β_1 and β_2) are indicated with blue arrows. For the $\left(\sqrt{3}\times\sqrt{3}\right)R30^\circ$ termination, the most stable adsorption structure (γ) is also the dissociation precursor state. Platinum atoms are represented in yellow, tin in green and oxygen in red. (For interpretation of the references to colour in this figure legend, the reader is referred to the web version of this article.)

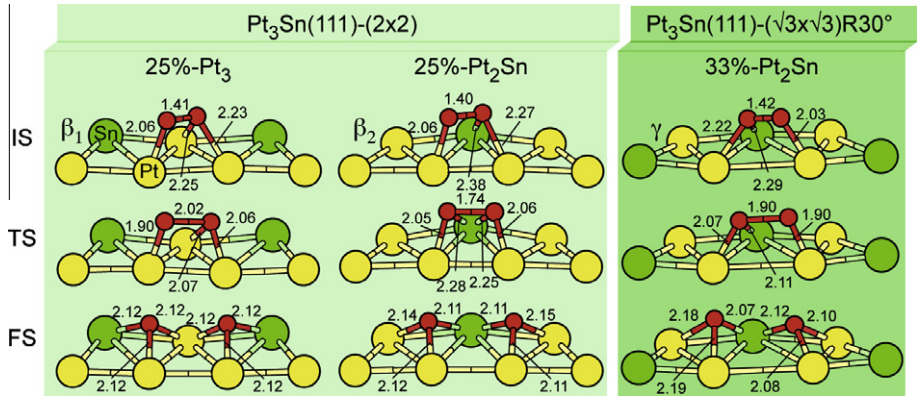

Fig. 5. Optimized structures for O_2 dissociation on $Pt_3Sn(1\,1\,1)$-(2×2) (25%-Pt_3 and 25%-Pt_2Sn) and on $Pt_3Sn(1\,1\,1)$-$\left(\sqrt{3}\times\sqrt{3}\right)R30^\circ$ (33%-Pt_2Sn). On the three surfaces, both surface tin content (25 or 33 at.%) and reactive site (Pt_3 or Pt_2Sn) change. For each pathway, the initial (IS), the transition (TS) and the final (FS) states are drawn for a low coverage ($\theta_{O_2} = 1/12$ ML). The relevant distances are reported in Å. Platinum atoms are represented in yellow, tin in green and oxygen in red. (For interpretation of the references to colour in this figure legend, the reader is referred to the web version of this article.)

Table 1
Molecular adsorption energy $E_{ads}^{O_2}$, dissociated state coadsorption energy E_{coads}^{O+O}, dissociation energy E_{diss}, activation energy E_{act}, zero-point energy (ZPE) corrected activation energy E_{act}^{ZPE}, effective activation energy E_{act}^{eff} including ZPE and diffusion energy, pre-exponential factor $k_{300\,K}^{0}$, rate constant $k_{300\,K}^{diss}$, effective dissociation rate constant $k_{300\,K}^{diss,eff}$ and the imaginary frequency ν^{im} for O_2 dissociation on $Pt_3Sn(1\,1\,1)$-(2×2) (25%-Pt_3, 25%-Pt_2Sn) and $\left(\sqrt{3}\times\sqrt{3}\right)R30^\circ$ (33%-Pt_2Sn). All energies are given in eV, rate constants in s^{-1} and imaginary frequency in cm^{-1}. These values correspond to a low coverage (1/12 ML). See Fig. 2 for definitions and Eq. (2).

Pathway	$E_{ads}^{O_2}$	E_{coads}^{O+O}	E_{diss}	E_{act}	E_{act}^{ZPE}	E_{act}^{eff}	$k_{300\,K}^{0}$	$k_{300\,K}^{diss}$	$k_{300\,K}^{diss,eff}$	ν^{im}
25%-Pt_3	−0.71	−2.36	−1.65	0.67	0.63	0.67	8.8×10^{12}	2.1×10^{2}	5.9×10^{1}	372i
25%-Pt_2Sn	−0.59	−2.55	−1.96	0.44	0.40	0.55	4.3×10^{12}	8.2×10^{5}	2.8×10^{3}	380i
33%-Pt_2Sn	−0.72	−1.60	−0.88	0.35	0.31	0.31	8.6×10^{12}	5.7×10^{7}	5.7×10^{7}	210i

almost symmetric TS with both oxygen atoms in direct interaction with one surface tin atom (bridge sites). From the energetic point of view, the 25%-Pt_3 pathway is less exothermic than 25%-Pt_2Sn (−1.65 eV against −1.96 eV). In agreement with the Hammond principle, the activation energy is larger for 25%-Pt_3 than for 25%-Pt_2Sn (0.67 eV against 0.44 eV). As a preliminary conclusion, the dissociation route involving the surface tin is preferential. This could be explained by a simple electronic reasoning. Indeed, the full Pt *d*-band is not favorable for coadsorbing several oxygen atoms, whereas the partially occupied Sn *sp*-band can stabilize such a structure. According to the optimized TS geometries, the O–O distance is shorter for 25%-Pt_2Sn (1.74 Å, earlier TS) than for 25%-Pt_3 (2.02 Å, later TS).

On the $\left(\sqrt{3}\times\sqrt{3}\right)R30^\circ$, the dissociation pathway resembles the best route on the (2×2) (25%-Pt_2Sn), since it occurs essentially on a similar Pt_2Sn site. However, subtle geometrical discrepancies appear, as depicted in Fig. 5. For 33%-Pt_2Sn, the dissociated final state is found non-symmetric regarding the relative height of the oxygen atoms (one exhibiting larger Pt–O distances than the other). Similarly, the corresponding TS is asymmetric (one oxygen being adsorbed on a top Pt position, the other on a bridge PtSn site). Indeed, tin depletion in the second layer induces different adsorption structures for FS and TS, by comparison with 25%-Pt_2Sn. From an energetic point of view, the dissociation is almost twice less exothermic for 33%-Pt_2Sn than for 25%-Pt_2Sn (−0.88 eV versus −1.96 eV, cf. Table 1). In contrast, the activation barrier is smaller on the $\left(\sqrt{3}\times\sqrt{3}\right)R30^\circ$ termination (0.35 eV compared to 0.44 eV). The larger stability of the final state for 25%-Pt_2Sn is addressed in Table 1 (−2.55 eV for the coadsorption state on (2×2) against −1.60 eV on $\left(\sqrt{3}\times\sqrt{3}\right)R30^\circ$). It is due mainly to a larger

oxophilic character of the surface interacting tin atom (in average, each surface tin interacts directly with more platinum atoms, so it presents a more depleted *sp*-band). This argument still holds for explaining the asymmetry observed at the TS. Regarding the corresponding optimal geometry, the O–O distance is longer (1.90 Å) for 33%-Pt_2Sn than for 25%-Pt_2Sn (1.74 Å). A last remark concerns the calculated imaginary frequencies of the best pathways on both terminations. A larger frequency is associated with a larger activation barrier (380i cm^{-1} for 25%-Pt_2Sn versus 210i cm^{-1} for 33%-Pt_2Sn).

Among the major aspects of this combined experimental and theoretical study, the theoretical kinetic analysis is important to interpret the measured catalytic activities and apparent barriers. The effective activation barriers E_{act}^{eff} and the dissociation rate constants $k_{300\ K}^{diss,eff}$ are reported in Table 1, the corresponding definition in Fig. 2. For the (2×2) surface, these calculated quantities include the diffusion thermodynamic process between the most stable (α) and the dissociation precursor states (β_1 and β_2). As a first remark, the correction due to diffusion does not change the energetic order between the three dissociation pathways. The pre-exponential factors obtained at 300 K are of the same order of magnitude, just below the classical value k_BT/h. Although the impact of the diffusion process on the barrier relative order is null, the change obtained on the effective barriers is significant, mainly for 25%-Pt_2Sn. As a consequence, the corresponding dissociation rate constant is different for this pathway by comparison with the effective rate constant (more than three orders of magnitude are lost for 25%-Pt_2Sn). The key point concerns the comparison between the best pathways on both terminations. According to the effective rate constants calculated at 300 K, the oxygen dissociation is almost four orders of magnitude more efficient on $\left(\sqrt{3} \times \sqrt{3}\right)$R30° than on (2×2). This outstanding result demonstrates the large ability of the $\left(\sqrt{3} \times \sqrt{3}\right)$R30° surface to dissociate molecular oxygen. This will have major implications in the following general discussion.

The remarkable activity of PtSn surfaces toward oxygen dissociation can be compared to previous theoretical results on Pt(1 1 1) [57–59]. Interestingly, the presence of tin in the catalytic site has a strong influence on the activation barrier. For instance, 25%-Pt_2Sn and 33%-Pt_2Sn pathways show an almost twice lower barrier (0.35–0.44 eV) than the one reported on Pt(1 1 1) by Kandoi et al. (0.77 eV at a higher coverage of 1/4 ML). The gain is less for 25%-Pt_3. Thus, PtSn catalyst offers a higher propensity for dissociating oxygen.

As an intermediate conclusion, the comparison of the three pathways indicates that tin plays a significant role at two different levels: the tin surface concentration and the chemical nature of the active site. Besides, on both terminations, molecular oxygen is expected to dissociate easily. Hence, this elementary process should not be the rate determining step for the complete CO oxidation reaction.

4.2. Carbon monoxide oxidation

As exposed before, carbon monoxide can be oxidized following either a concerted mechanism occurring with molecular oxygen or a stepwise process involving atomic oxygen. Both routes have been explored here on the two terminations of the Pt_3Sn(1 1 1) alloy. According to previous analysis on Pt(1 1 1) [56], the oxidation following a bimolecular concerted mechanism between CO and O_2 is preferential only at low coverage because of the required space to adsorb all the intermediates. Likewise, our analysis is detailed for a low coverage situation (1/12 ML).

The major results coming from our DFT approach regarding the concerted process show that the activation energy barrier ranges from 0.49 eV on the (2×2) termination to 0.59 eV on the $\left(\sqrt{3} \times \sqrt{3}\right)$R30° surface (see the Supplementary information for all the details about energetics and adsorption structures). These values should be compared to the calculated barriers obtained for oxygen dissociation on the two surfaces: 0.44 and 0.35 eV, respectively. Thus, even at low coverage, the activation barriers for the concerted mechanism are higher than those of the direct oxygen dissociation, whatever the surface tin content. This original result contrasts with the case of Pt(1 1 1) [56]. In the following, we will thus focus our efforts on the second oxidation mechanism involving atomic oxygen. This stepwise process has been addressed previously at a higher coverage on the Pt(1 1 1) and the Pt_3Sn(1 1 1)-(2×2) surfaces ($\theta_{CO} = \theta_O = 1/4$ ML) [40]. Here, we present new results related to the influences of coverage and surface tin content on activation barriers and kinetic properties. To be consistent with oxygen dissociation results, energetics and kinetics are summarized in Table 2 at coverage 1/12 ML, while the details of the reaction pathways are exposed in the Supplementary information.

Coverage effect is straightforward. When the coverage decreases from 1/4 ML to 1/12 ML, the initial coadsorption states between CO and O, before oxidation, are systematically stabilized on the three considered surfaces (Pt(1 1 1), Pt_3Sn(1 1 1)-(2×2) and Pt_3Sn(1 1 1)-$\left(\sqrt{3} \times \sqrt{3}\right)$R30°)). This leads clearly to a loss of exothermicity for the oxidation reaction. Regarding the activation barrier, this corresponds to an increase of 0.1 eV for Pt(1 1 1) and 0.18 eV for Pt_3Sn(1 1 1)-(2×2) (see Table 2 for 1/12 ML and Ref. [40] for 1/4 ML). Consequently, a significant decrease of the oxidation rate constant is noticed (a loss of approximately two orders of magnitude for the rate constants between 1/4 and 1/12 ML at 300 K).

The influence of surface tin content is also clear-cut. Due to a strong destabilization of the initial coadsorbed state, the exothermicity of the oxidation step increases with the surface tin concentration, while the activation barrier decreases accordingly. At this stage of the discussion, the most active surface regarding carbon monoxide oxidation is Pt_3Sn(1 1 1)-$\left(\sqrt{3} \times \sqrt{3}\right)$R30° with a barrier of 0.68 eV and a rate constant of 3.4×10^{-2} ML^{-1} s^{-1}. However, this rate cannot compete with oxygen dissociation rates which are faster by several orders of magnitude whatever the considered surface, according to Table 1. Hence, at low coverage, carbon monoxide oxidation appears to be the rate determining step of the complete mechanism. This argumentation will be developed in the next section.

5. Discussion

According to the theoretical analysis of reaction pathways and kinetics at low coverage, the two tailored terminations of the Pt_3Sn(1 1 1) surface exhibit an outstanding catalytic activity regarding oxygen dissociation at room temperature. Besides, kinetic measurements provided here support that the PtSn alloy offers a much better activity than pure Pt for carbon monoxide oxidation.

In the following, the interpretation of the measurements will be sketched from DFT results obtained at low oxygen coverage. In order to evaluate how far this analysis is valid, the modifications coming from the increase in oxygen coverage will be explored by considering it as a perturbation. Since the experimental coverage is unknown, theory is used as a guide to advance in the discussion.

Moreover, under elevated pressure, the structure and the modifications of the catalyst are not available yet. For instance, the existence and the formation of surface oxides are still an open question, in particular during the reaction. As a first insight, our theoretical efforts have hence been focussed on tailored non-oxidized alloy surfaces.

Finally, the mediatory role of tin will be illustrated by a charge transfer analysis in the last section of the discussion.

Table 2
Coadsorption energy E_{coads}^{CO+O}(eV), adsorption energy of CO_2 $E_{ads}^{CO_2}$ (eV), oxidation energy E_{oxi} (eV), oxidation activation energy E_{act} (eV), zero-point energy (ZPE) corrected activation barrier E_{act}^{ZPE} (eV), pre-exponential factor $k_{300\ K}^{0}$ ($ML^{-1}\ s^{-1}$), oxidation rate constant $k_{300\ K}^{oxi}$ ($ML^{-1}\ s^{-1}$) at 300 K and the imaginary frequency v^{im} for CO oxidation on $Pt_3Sn(1\,1\,1)$-(2×2) (25%-Pt_2Sn), $Pt_3Sn(1\,1\,1)$-$\left(\sqrt{3}\times\sqrt{3}\right)R30^\circ$ (33%-Pt_2Sn) and Pt(1 1 1). These values correspond to a low coverage of 1/12 ML.

	E_{coads}^{CO+O}	$E_{ads}^{CO_2}$	E_{oxi}	E_{act}	E_{act}^{ZPE}	$k_{300\ K}^{0}$	$k_{300\ K}^{oxi}$	v^{im}
Pure Pt	−3.15	0.02	−0.08	0.92	0.89	5.5×10^{9}	6.4×10^{-6}	320i
25%-Pt_2Sn	−2.82	0.26	−0.17	0.86	0.83	8.0×10^{9}	7.7×10^{-5}	307i
33%-Pt_2Sn	−2.39	0.28	−0.59	0.68	0.66	4.9×10^{9}	3.4×10^{-2}	281i

5.1. Oxygen coverage analysis

Experimental measurements have shown that the $Pt_3Sn(1\,1\,1)$-(2×2) termination is more efficient than the $\left(\sqrt{3}\times\sqrt{3}\right)R30^\circ$ surface for carbon monoxide oxidation. In order to interpret this activity change theoretically, the energy profiles related to oxygen dissociation followed by carbon monoxide oxidation are assembled in Fig. 6 for these PtSn surfaces.

As a first comment, the energetic profile corresponding to the (2×2) is composed of intermediate states either more stable than those of the $\left(\sqrt{3}\times\sqrt{3}\right)R30^\circ$ or as stable as these latter ones. This results essentially from the CO adsorption state which is more stable on the (2×2). Since the oxygen dissociation transition states exhibit the same stability, the corresponding barrier is larger on the (2×2). Nevertheless, the barriers are sufficiently small to ensure that oxygen dissociation is never the rate determining step, whatever the surface tin content. This argument is supported by rate constants calculated at 300 K. Therefore, the experimental activity differences could be explained by the theoretical analysis focused on the carbon monoxide oxidation.

According to the energy profiles, the effective activation barriers including the coadsorption energetic cost are similar (0.96 eV for the (2×2) and 0.95 eV for the $\left(\sqrt{3}\times\sqrt{3}\right)R30^\circ$). At this stage, the discussion at low oxygen coverage does not solve the key questions of activity changes for PtSn surfaces. Nonetheless, the activation barriers on Pt(1 1 1) (0.92 eV at 1/12 ML and 0.82 eV at 1/4 ML [40]) are higher than those on Pt_3Sn-(2×2) (0.86 eV at 1/12 ML and 0.68 eV at 1/4 ML [40]). This is fully compatible with the lowering of the apparent activation barrier observed experimentally.

This argumentation needs to be modulated by considering the perturbation on the activation barriers resulting from the increase in oxygen coverage. The corresponding results are exposed in Fig. 7 for energetics and in the Supplementary information for all the detailed structures. The barriers are determined from the previous reaction pathways (oxygen dissociation and carbon monoxide oxidation) by coadsorbing oxygen atoms in the supercells, as far as possible from the active site. These additional oxygen atoms are named spectators since they are not directly involved in the mechanisms. Their number ranges from zero (previously exposed low coverage case) to two atoms in the supercell (0.17 ML), giving in practice a small coverage variation and a controlled perturbation of the surface. According to our previous analysis of atomic oxygen adsorption [48], this restriction is imposed by the formation of tin-oxide units on the surface, already at a medium coverage (see the Supplementary information for details). Regarding the oxygen dissociation, the picture remains intact. Both PtSn terminations exhibit small barriers which slightly vary with oxygen coverage (see Fig. 7). Here again, in this range of coverage, oxygen dissociation is not the rate determining step on PtSn alloy surfaces. Concerning now the carbon monoxide oxidation, the situation has changed, clearly for the (2×2). Indeed, the small increase in oxygen coverage induces a decrease of the barrier. This result is fully compatible with our previous high coverage situation [40]. So the activity gain observed between pure Pt and PtSn surfaces can be explained by this higher coverage analysis. Nonetheless, the discrepancies measured on the PtSn surfaces are not elucidated by this theoretical model. Among the assumptions allowing a better description, the consideration of surface oxidation appears priority.

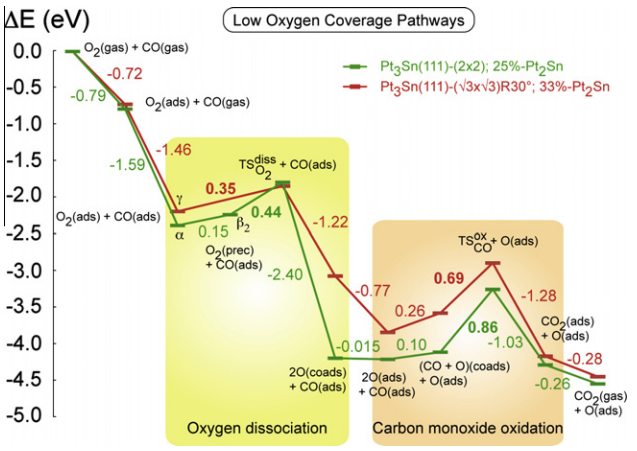

Fig. 6. Energy profiles (eV) of oxygen dissociation and carbon monoxide oxidation competitive pathways on the two terminations of $Pt_3Sn(1\,1\,1)$ at an oxygen coverage of 1/12 ML. The references are the clean surfaces, and the molecular oxygen and carbon monoxide gas phases.

5.2. Mediatory role of tin

In the following, the specific role of tin in the alloy is discussed from a charge transfer analysis of oxygen dissociation on the $Pt_3Sn(1\,1\,1)$ surfaces. This electronic transfer is illustrated by a charge variation at the transition-state structures (plane wave basis set with VASP) and by a Mulliken atomic charge variation (localized basis sets with DMol3, as detailed in the Supplementary information). On top of Fig. 8, the charge transfer is calculated by the difference between the total electronic density at the TS structure and the densities of the metal and the adsorbate separated fragments at the same geometry. On bottom of Fig. 8, the atomic charge variations are calculated between initial and transition-state structures. Conceptually, the alloy catalyst is divided into four blocks associated with the different surface (top), bulk (bottom), platinum (left) and tin (right) atoms. In each block, the variations are summed over all the corresponding atoms.

On the (2×2), the 25%-Pt_3 pathway, where the active site is composed of platinum atoms, serves as the reference. At the TS, the dissociation of the O–O bond induces a charge redistribution between oxygen and platinum atoms (blue region). The oxygen atoms have lost some electronic density by comparison with isolated oxygen references. Moreover, the chemical bonding between Pt and O occurs through $5d_{z^2}$ atomic orbitals for Pt and $2p$ atomic orbitals for O. Regarding the Mulliken charge variations, the oxygen atoms acquire a substantial additional electronic density (−0.35 electron) between the initial and the transition states. This negative charge is compensated mainly by the bulk platinum (0.28 electron). Tin atoms are almost neutral (0.11 electron in the surface plane and 0.02 electron in the bulk).

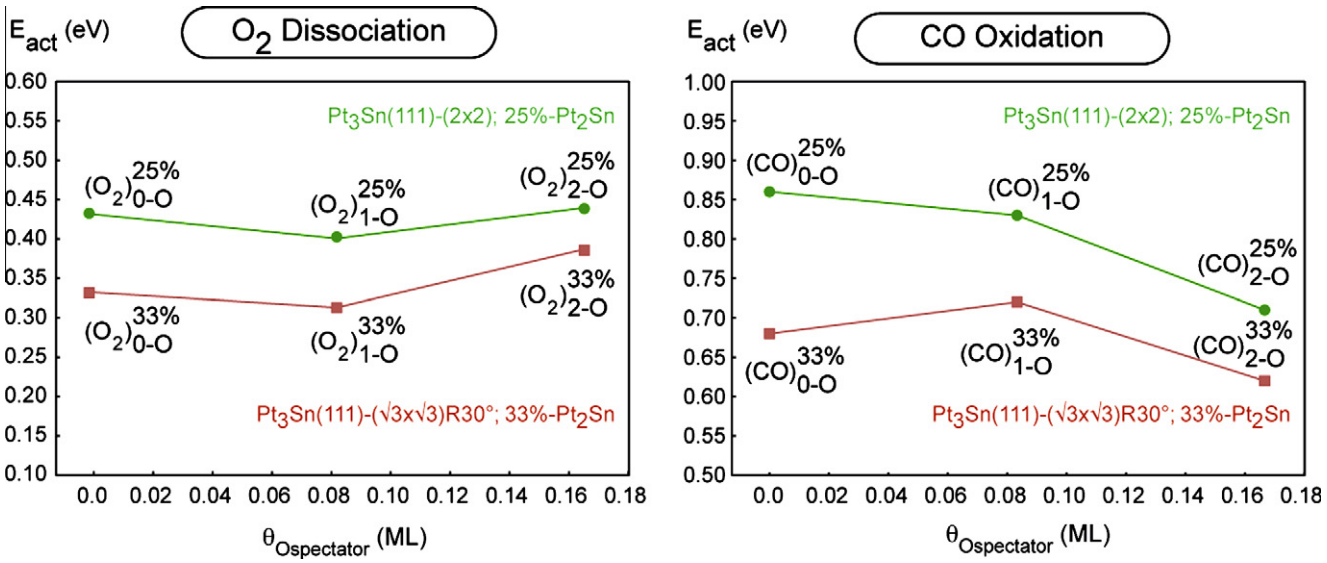

Fig. 7. Influence of oxygen coverage (ML) on the activation energy barrier of oxygen dissociation and carbon monoxide oxidation on $Pt_3Sn(111)$-(2×2) and $Pt_3Sn(111)$-$\left(\sqrt{3} \times \sqrt{3}\right)R30^\circ$. Activation energy ($E_{act}$) is reported in eV. $\theta_{O\ spectator}$ takes into account only the supplementary oxygen atoms added on the surface.

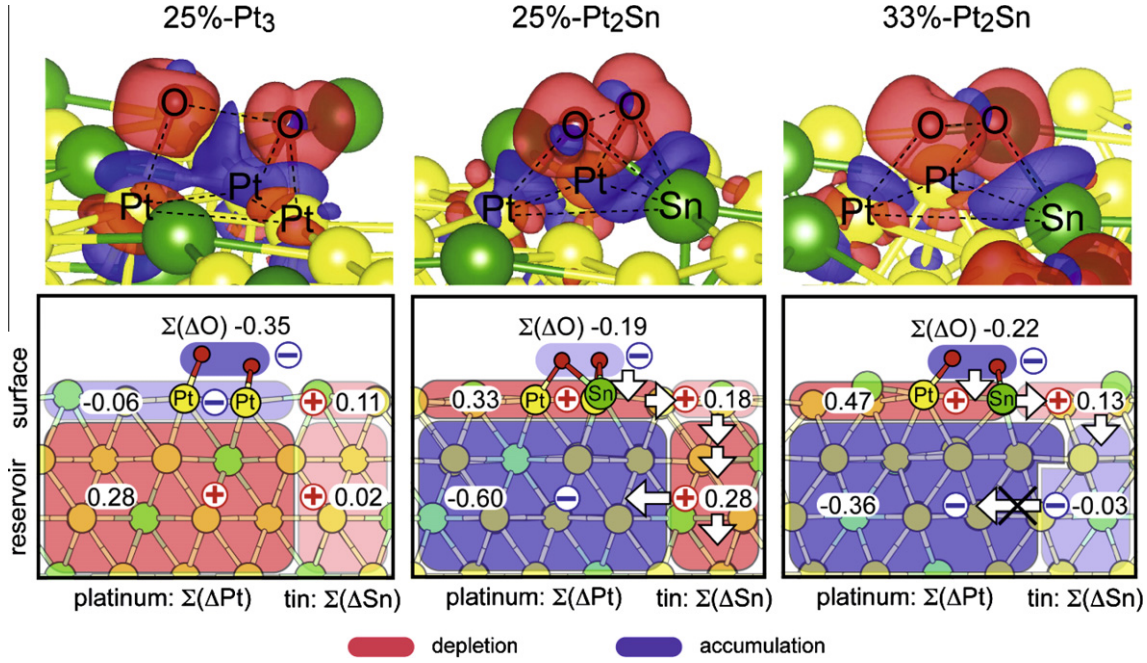

Fig. 8. Top: charge transfer at the transition-state structures calculated with plane wave basis sets for O_2 dissociation pathways on $Pt_3Sn(111)$-(2×2) (25%-Pt_3 and 25%-Pt_2Sn) and on $Pt_3Sn(111)$-$\left(\sqrt{3} \times \sqrt{3}\right)R30^\circ$ (33%-Pt_2Sn) (see Fig. 5 for the optimized geometries). Bottom: atomic charge variations calculated with localized basis sets between the dissociation precursor states and the transition states. The alloy system is conceptually divided into four blocks: surface (top), bulk (bottom), platinum (left) and tin (right) atoms. For each block and for the oxygen atoms, the summed charge variations are indicated. The white arrows show the electronic transfer mediated by tin.

When the oxygen dissociation involves one surface tin atom (25%-Pt_2Sn), the picture is deeply modified. At the TS, the charge redistribution on the metal surface atoms is different. The Pt $5d_{z^2}$ orbitals exhibit a weaker density, and the Sn 5*sp* orbitals are almost non-perturbed by the adsorbates, although there exists a region with a charge accumulation between oxygen atoms and tin. Concerning the Mulliken charge variations, the oxygen atoms gain less electron (−0.19 electron) between initial and transition states. This electronic loss is compensated by a strong charge accumulation in the platinum bulk (−0.60 electron), completely mediated by surface (0.18 electron) and bulk (0.28 electron) tin atoms. The surface platinum atoms participate to this phenomenon, to a lower extent (0.33 electron). This strong mediatory effect of tin impacts directly on the decrease of the activation barrier (0.67 eV for 25%-Pt_3 against 0.44 eV for 25%-Pt_2Sn). The observed strong charge redistribution is an original phenomenon. Indeed, the surface tin atom involved in the active site governs the filling of the electronic reservoir related to the alloy bulk.

On the $\left(\sqrt{3} \times \sqrt{3}\right)R30^\circ$, the picture for 33%-$Pt_2Sn$ is similar to 25%-Pt_2Sn. The stoichiometry perturbation between the surface and the second layer slightly modulates the phenomenon. The tin depletion in the second plane is responsible for the decrease of the mediatory effect. The major change appears on the Pt bulk reservoir, the charge of which is significantly lowered (−0.36 electron).

In that case, the layer-by-layer tin charge transfer is simply switched off (−0.03 electron).

6. Conclusion

In the present study, we have demonstrated the mediatory role of tin in the $Pt_3Sn(1\,1\,1)$ surfaces for activating oxygen, from comprehensive experimental and theoretical approaches. From kinetic measurements in the range 300–425 K and under elevated pressure of reactants, the $Pt_3Sn(1\,1\,1)$-(2×2) and $\left(\sqrt{3}\times\sqrt{3}\right)R30^\circ$ surfaces are more active for carbon monoxide oxidation than the $Pt(1\,1\,1)$ reference catalyst. The (2×2) shows systematically a larger catalytic activity than the $\left(\sqrt{3}\times\sqrt{3}\right)R30^\circ$. The lowering of the apparent activation barrier (from 0.57 eV for $Pt(1\,1\,1)$ to 0.30 eV for $Pt_3Sn(1\,1\,1)$-(2×2)) is emphasized by a gain of several orders of magnitude regarding the rate constants under these operating conditions.

The kinetic experimental investigation is supported by a detailed theoretical analysis. This approach demonstrates that oxygen dissociation is never the rate determining step of the reaction. The activation energy is low and is slightly modified by the surface tin concentration (0.35–0.44 eV) and by the oxygen coverage (0.32–0.45 eV). The PtSn surfaces exhibit a much lower activation barrier than the one proposed previously on $Pt(1\,1\,1)$ (0.77 eV [59]). Regarding carbon monoxide oxidation, higher activation energies are calculated on the PtSn alloys (0.68–0.86 eV at 1/12 ML). However, these values are lower than the barrier on $Pt(1\,1\,1)$ (0.92 eV at 1/12 ML), in agreement with our experimental apparent activation energies.

The role of tin has been illustrated by a charge transfer analysis. The associated electronic phenomenon corresponds to a layer-by-layer charge transfer mediated by tin from adsorbed oxygen to bulk platinum, acting as an electron reservoir. The surface intermediates are more stable when the transfer is switched on. The effect is all the more efficient since the species is stable. In the case of PtSn surfaces, the activation barrier order has been explained by this mediatory phenomenon. In particular, the specific role of active sites involving one tin atom has been emphasized by comparison with pure Pt active sites.

Although the outstanding ability of PtSn catalysts for activating oxygen has been evidenced clearly, the performance discrepancies observed experimentally between the two terminations are not elucidated at this stage. The joint experimental and theoretical analyses have allowed the exclusion of several mechanistic assumptions and have opened the discussion of the exact nature of the catalyst surface under realistic conditions. In fact, this study raises the question of a possible surface oxide formation prior carbon monoxide oxidation.

Acknowledgments

The authors thank IDRIS at Orsay, CINES at Montpellier and PSMN at Lyon, for CPU time and assistance (project 609). They acknowledge PHC PROCOPE and ANR SIRE contract for financial support. They thank also Professor Ugo Bardi (Universita di Firenze, Italy) for the loan of his $Pt_3Sn(1\,1\,1)$ sample.

Appendix A. Supplementary data

In the supplementary material, the equations, which are used in the experimental section for the calculation of the catalytic activity and turnover frequency, are exposed in more details. In addition, the theoretical results regarding the optimized structures involved in oxygen dissociation and carbon monoxide oxidation on PtSn surfaces are presented comprehensively and commented. Finally, the complete Mulliken atomic charge analysis is reported. Supplementary data associated with this article can be found, in the online version, at doi:10.1016/j.jcat.2010.05.014.

References

[1] H. Arakawa, M. Aresta, N. Armor, M.A. Barteau, E.J. Beckman, A.T. Bell, J.E. Bercaw, C. Creutz, E. Dinjus, D.A. Dixon, K. Domen, D.L. DuBois, J. Eckert, E. Fujita, D.H. Gibson, W.A. Goddard, D.W. Goodman, J. Keller, G.J. Kubas, H.H. Kung, J.E. Lyons, L.E. Manzer, T.J. Marks, K. Morokuma, K.M. Nicholas, R. Periana, L. Que, J. Rostrup-Nielson, W.M.H. Sachtler, L.D. Schmidt, A. Sen, G.A. Somorjai, P.C. Stair, B.R. Stults, W. Tumas, Chem. Rev. 101 (2001) 953.
[2] M. Haruta, Nature 437 (2005) 1098.
[3] W.L. Yim, T. Klüner, J. Catal. 254 (2008) 349.
[4] V.R. Stamenkovic, B. Fowler, B.S. Mun, G. Wang, P.N. Ross, C.A. Lucas, N.M. Markovic, Science 315 (2007) 493.
[5] V.R. Stamenkovic, B.S. Mun, K.J.J. Mayrhofer, P.N. Ross, N.M. Markovic, J. Am. Chem. Soc. 128 (2006) 8813.
[6] Z. Shi, PEM fuel cell electrocatalysts and catalyst layers, fundamentals and applications, in: Applications of First-Principles Methods in the Study of Fuel Cell Air-Cathode Electrocatalysis, Springer, 2008 (Chapter V).
[7] H. Over, A. Seitsonen, Science 297 (2002) 2003.
[8] H. Over, M. Muhler, Prog. Surf. Sci. 72 (2003) 3.
[9] M.D. Ackermann, T.M. Pedersen, B.L.M. Hendriksen, O. Robach, S.C. Bobaru, I. Popa, C. Quiros, H. Kim, B. Hammer, S. Ferrer, J.W.M. Frenken, Phys. Rev. Lett. 95 (2005) 255505.
[10] E. Lundgren, A. Mikkelsen, J.N. Andersen, G. Kresse, M. Schmid, P. Varga, J. Phys.: Condens. Matter 18 (2006) R481.
[11] J. Klikovits, E. Napetschnig, M. Schmid, N. Seriani, O. Dubay, G. Kresse, P. Varga, Phys. Rev. B 76 (2007) 045405.
[12] J. Gustafson, R. Westerström, A. Resta, A. Mikkelsen, J. Andersen, O. Balmes, X. Torrelles, M. Schmid, P. Varga, B. Hammer, G. Kresse, C. Baddeley, E. Lundgren, Catal. Today 145 (2009) 227.
[13] K. Reuter, M. Scheffler, Phys. Rev. Lett. 90 (2003) 046103.
[14] K. Reuter, D. Frenkel, M. Scheffler, Phys. Rev. Lett. 93 (2004) 116105.
[15] K. Reuter, M. Scheffler, Phys. Rev. B 73 (2006) 045433.
[16] M. Rieger, J. Rogal, K. Reuter, Phys. Rev. Lett. 100 (2008) 016105.
[17] A. Eichler, F. Mittendorfer, J. Hafner, Phys. Rev. B 62 (2000) 4744.
[18] Y. Xu, A.V. Ruban, M. Mavrikakis, J. Am. Chem. Soc. 126 (2004) 4717.
[19] M.T.M. Koper, T.E. Shubina, R.A. van Santen, J. Phys. Chem. B 106 (2002) 686.
[20] P. Liu, A. Logadottir, J.K. Nørskov, Electrochim. Acta 48 (2003) 3731.
[21] T.J. Schmidt, Z. Jusys, H.A. Gasteiger, R.J. Behm, U. Endruschat, H. Boennemann, J. Electrochem. Soc. 501 (2001) 132.
[22] M.M. Schubert, M.J. Kahlich, G. Feldmeyer, M. Huttner, S. Hackenberg, H.A. Gasteiger, R.J. Behm, Phys. Chem. Chem. Phys. 3 (2001) 1123.
[23] V.R. Stamenkovic, M. Arenz, C.A. Lucas, M.E. Gallagher, P.N. Ross, N.M. Markovic, J. Am. Chem. Soc. 125 (2003) 2736.
[24] N.M. Markovic, P.N. Ross, Surf. Sci. Rep. 45 (2002) 117.
[25] C. Dupont, D. Loffreda, F. Delbecq, F.J.C.S. Aires, E. Ehret, Y. Jugnet, J. Phys. Chem. C 112 (2008) 10862.
[26] F. Gao, Y. Wang, D.W. Goodman, J. Phys. Chem. C 113 (2009) 14993.
[27] F. Gao, Y. Wang, Y. Cai, D.W. Goodman, J. Phys. Chem. C 113 (2009) 174.
[28] H.A. Gasteiger, N.M. Markovic, P.N. Ross, Catal. Lett. 36 (1996) 1.
[29] S.M. McClure, D.W. Goodman, Chem. Phys. Lett. 469 (2009) 1.
[30] J. Greeley, J.K. Nørskov, Surf. Sci. 592 (2005) 104.
[31] E. Christoffersen, P. Liu, A. Ruban, H.L. Skriver, J.K. Nørskov, J. Catal. 199 (2001) 123.
[32] B. Hammer, J.K. Nørskov, Surf. Sci. 343 (1995) 211.
[33] F. Delbecq, P. Sautet, J. Catal. 220 (2003) 115.
[34] Z. Ji, J.Q. Li, Chem. Phys. Lett. 424 (2006) 111.
[35] C.J. Zhang, R.J. Baxter, P. Hu, A. Alavi, M.H. Lee, J. Chem. Phys. 115 (2001) 5272.
[36] J. Zhang, H. Jin, M. Sullivan, F.C.H. Lim, Phys. Chem. Chem. Phys. 11 (2009) 1441.
[37] J.K. Nørskov, J. Rossmeisl, A. Logadottir, L. Lindqvist, J.R. Kitchin, T. Bligaard, H. Jónsson, J. Phys. Chem. B 108 (2004) 17886.
[38] A. Staykov, T. Kamachi, T. Ishihara, K. Yoshizawa, J. Phys. Chem. C 112 (2008) 19501.
[39] S. Desai, M. Neurock, Electrochim. Acta 48 (2003) 3759.
[40] C. Dupont, Y. Jugnet, D. Loffreda, J. Am. Chem. Soc. 128 (2006) 9129.
[41] L.J. Shorthouse, Y. Jugnet, J.C. Bertolini, Catal. Today 70 (2001) 33.
[42] S. Speller, U. Bardi, The chemical physics of solid surfaces, Surface Alloys and Alloy Surfaces: The Platinum–Tin System, vol. 10, Elsevier, 2002 (Chapter IV).
[43] J. Kuntze, S. Speller, W. Heiland, A. Atrei, I. Spolveri, U. Bardi, Phys. Rev. B 58 (1998) R16005.
[44] G. Kresse, J. Hafner, Phys. Rev. B 47 (1993) 558.
[45] G. Kresse, J. Furthmller, Phys. Rev. B 54 (1996) 11169.
[46] J.P. Perdew, K. Burke, M. Ernzerhof, Phys. Rev. Lett. 77 (1996) 3865.
[47] G. Kresse, D. Joubert, Phys. Rev. B 59 (1999) 1758.
[48] C. Dupont, Y. Jugnet, F. Delbecq, D. Loffreda, J. Chem. Phys. 130 (2009) 124716.
[49] G. Henkelman, B.P. Uberuaga, H. Jonsson, J. Chem. Phys. 113 (2000) 9901.
[50] G. Henkelman, H. Jonsson, J. Chem. Phys. 113 (2000) 9978.
[51] B. Delley, J. Chem. Phys. 113 (2000) 7756.
[52] A. Atrei, U. Bardi, G. Rovida, M. Torrini, M. Hoheisel, S. Speller, Surf. Sci. 526 (2003) 193.

[53] C. Dupont, D. Loffreda, F. Delbecq, Y. Jugnet, J. Phys. Chem. C 111 (2007) 8524.
[54] M. Kinne, T. Fuhrmann, J.F. Zhu, C.M. Whelan, R. Denecke, H.P. Steinruck, J. Chem. Phys. 125 (2004) 7113.
[55] C. Hardacre, R.M. Ormerod, R.M. Lambert, Chem. Phys. Lett. 206 (1993) 171.
[56] A. Eichler, J. Hafner, Phys. Rev. B 59 (1999) 5960.
[57] A. Eichler, J. Hafner, Phys. Rev. Lett. 79 (1997) 4481.
[58] P. Gambardella, Z. Sljivancanin, B. Hammer, M. Blanc, K. Kuhnke, K. Kern, Phys. Rev. Lett. 87 (2001). 056103-1.
[59] S. Kandoi, A.A. Gokhale, L.C. Grabow, J.A. Dumesic, M. Mavrikakis, Catal. Lett. 93 (2004) 93.